Materials and Structures (2016) 49:3293–3308
DOI 10.1617/s11527-015-0720-5

ORIGINAL ARTICLE

In-plane cyclic behaviour of unfired clay and earth brick walls in both unstrengthened and strengthened conditions

Stanislav Hračov · Stanislav Pospíšil · Angelo Garofano · Shota Urushadze

Received: 20 January 2014 / Accepted: 28 September 2015 / Published online: 14 October 2015

Abstract This article presents the outcome of a series of in-plane shear tests on non-traditional masonry walls under unstrengthened and strengthened conditions. The uniqueness of the experiments arises from the testing of unfired clay and earth (adobe) bricks, which are typical for numerous historical buildings and which have significantly different mechanical properties in comparison with the nowadays commonly used fired bricks, concrete blocks, etc. The applicability and suitability of two different strengthening techniques, which do not require significant structural intervention, were investigated with the use of two evaluation procedures. The first technique was realised using steel wire ropes that were mechanically fastened to the wall and arranged in an X shape. The other technique comprised of the application of a geo-net to the surface of the wall, which was then covered with a layer of adobe plaster. Two different types of geo-nets were tested. The paper focuses on the assessment of the influences of both strengthening techniques in changing the structural resistance of the walls loaded by a combination of constant vertical compression and a cyclic horizontal loading. Other mechanical parameters, e.g. ductility or damping, were also investigated in detail. In addition, the geo-net retrofitting technique applied to a previously damaged wall was studied. Conclusions and practical recommendations for preventive strengthening of adobe and dry brick masonry walls or for remedial work on damaged masonry in regions with high seismic risk are given.

Keywords Seismic strengthening · Retrofitting · Earth brick walls · Experimental tests · Energy dissipation · Earthquake engineering

S. Hračov (✉) · S. Pospíšil · S. Urushadze
Institute of Theoretical and Applied Mechanics AS CR, v.v.i., Prague, Czech Republic
e-mail: hracov@itam.cas.cz

S. Pospíšil
e-mail: pospisil@itam.cas.cz

S. Urushadze
e-mail: urushadze@itam.cas.cz

A. Garofano
Applied Computing and Mechanics Laboratory, École Polytechnique Fédérale de Lausanne, Lausanne, Switzerland
e-mail: angelo.garofano@epfl.ch

1 Introduction

Much of the architectural heritage in the regions of the world with high seismic activity was built from dried earthen materials such as unfired clay and adobe bricks. It is estimated that approximately 30 % of the world's population lives in earth buildings [1, 2]. Especially in the developing countries the earthen built heritage is very important and comprises of simple houses in rural areas as well as important

monuments. However, this type of construction raises concerns about the structural performance during earthquakes. As a result, the definition of preventive measures and adequate low cost seismic strengthening techniques represents a key aspect in the conservation of this particular type of built heritage.

Structurally, soil as a building material performs well against compression forces but has a low tensile strength, see e.g. [3]. Therefore it is important to adjust the structural elements made with this material towards compression and to transfer the majority of the tensile forces that occur during earthquakes [4] to the strengthening elements. The choice of the strengthening system depends on the type of structure and should be properly calibrated with respect to the failure mechanisms, the overall ductility and the energy dissipation. Masonry elements have been strengthened for many centuries by traditional methods involving, for example, filling of cracks or voids by grouting, stitching of large cracks or other weak areas with metallic elements or concrete, application of strengthened grouted perforations, etc. All these traditional techniques are, however, limited by some disadvantages that restrict their application [5], which has prompted researchers to develop more adequate and effective solutions. The use of materials such as concrete cement and steel elements for the strengthening and retrofitting of masonry structures revealed disadvantages in relation to the reduction of available space, architecture impact, heavy mass, corrosion potential, employment of organic binders etc. Therefore, new methods need to be applied using new materials and technology.

One of the early studies on the use of non-metallic reinforcement for strengthening of masonry walls was realised with vertical or inclined low-modulus polypropylene braids, see [6]. The concepts and analytic results regarding the applicability and effectiveness of fibre reinforced polymeric (FRP) tendons used to apply circumferential pre-stressing to historic masonry structures were given by [7] and [8]. The FRP overlays have also been applied to strengthen walls, see for example [9]. [10] investigated the use of carbon laminates (CFRP) as non-seismic strengthening elements of masonry structures. The studies [11] and [12] focused on experimental investigations, involving quasi-static tests of unreinforced masonry specimens strengthened with epoxy-bonded glass fabrics. For the strengthening of the masonry walls subjected to in-plane and out-of-plane cyclic loading, textile reinforced mortar (TRM), characterised by high compatibility with the substrate, was proposed by [13, 14] and [15]. [16] employed a similar technique consisting of a carbon mesh arranged bi-directionally and placed within two layers of mortar in order to strengthen yellow-tuff-masonry walls. Over the last few years polymer resins have been substituted by cement or lime based mortars. The use of inorganic materials as a binder can be more effective than the use of organic resin if the thermo-hygrometric aspects are taken into account, see [17]. In [18] a composite system consisting of a sequence of layers of cement-based matrix and alkali resistant glass coated reinforcing grids was successfully tested.

The present work describes the employment of geonets and wire ropes as a strengthening technique for masonry walls. Both methods take advantage of the well-known benefits of these materials, such as their mechanical properties, high strength to weight ratio, high resistance to corrosion in comparison with other metallic strengthening systems, ease of application and the preservation of the geometrical and, to some extent, also the architectural detail. The study is focused on the investigation of the mechanical behaviour of these particular strengthening systems in combination with unfired earth and clay masonry walls. The main interest is related to the improvements of the in-plane behaviour of the wall that are caused by the application of these strengthening methods.

2 Experimental procedure

2.1 Material and specimen specification

Experimental tests were carried out on two types of masonry panels, which differed in the structural materials used. Four panels were constructed using unfired ready-made adobe (earth) bricks and for a further four panels unfired classical clay bricks were used. The Flemish bond was used for the construction of all the panels. The adobe bricks [19] were produced by a mechanised hand moulding procedure without any compression and the unfired clay bricks were manufactured using a classical machine procedure typical for extruded fired brick. Both types of bricks had a dimensions of 240 × 115 × 71 mm. An overview of the physical and mechanical properties of

the bricks is given in Table 1. These figures were specified either by the manufacturer or determined in previously performed tests [20]. According to this reference, the Young's modulus $E_{1/3}$ was determined as a secant-modulus of the stress at a third of the compressive strength. Both types of bricks were bound with adobe mortar having similar physical and mechanical properties as adobe bricks, see Table 1. The overall dimensions of all tested walls were 240 mm in thickness, 1050 mm in width and 1367 mm in height.

2.2 Intervention techniques

Two different intervention techniques were applied in order to achieve an effective increase in the mechanical performance of the walls.

The first strengthening method was based on the application of a polyethylene (PET) [21] and polypropylene geo-nets (PP) [22] onto both sides of the wall. The geo-nets that were chosen are both commonly available and affordable and are normally used either as anti-cracking nets for plaster reinforcement (PP) or are suitable for sub-grade stabilization and base reinforcement applications (PET). The basic mechanical properties and a detailed picture of the geo-nets are given in Table 2 and in Fig. 1, respectively. The shear stiffness in Table 2 expresses the differences in plane rigidity between the geo-nets. It is expressed as the force required to cause a 1 % drift of one row of mesh of a 1 m long geo-net. The PET geo-net, contrary to the PP geo-net, had almost zero shear stiffness.

The geo-nets were attached by means of steel staples applied with a pneumatic pistol. The U-shaped staples were positioned according to a grid with dimensions of 150 mm × 70 mm and were embedded into the bricks to a depth of 10 mm. After the mechanical fastening of the geo-nets to the surfaces, the walls were covered with an adobe plaster of about 20 mm in thickness, see Fig. 2 (left). In the case of the unfired clay brick wall with the PP geo-nets, the surface was not plastered in order to determine the influence of the plaster on the overall mechanical behaviour. The PET geo-nets were also applied to a previously damaged unstrengthened adobe wall which was tested for the purpose of retrofitting.

The second intervention method was represented by the application of three steel wire ropes placed along each diagonal of both sides of the wall, see Fig. 2 (right), thereby strengthening the undamaged masonry

Table 1 Material specifications of bricks and mortar [20]

Title	Density ϱ (kg m^{-3})	Compressive strength f (MPa)		Tensile strength f (MPa)		Young's modulus $E_{1/3}$ (GPa)		Poisson's ratio ν (/)	
	Mean	Mean	STD	Mean	STD	Mean	STD	Mean	STD
Adobe brick	1870	5.10	0.31	0.50	0.14	2.20	0.1	0.43	0.07
Unfired clay brick	1900	7.50	0.28	0.82	0.12	3.20	0.1	0.45	0.08
Adobe mortar	1900	3.16	0.44	0.30	0.08	1.07	0.2	–	–
Adobe brick masonry	1890	3.28	0.40	–	–	0.80	0.2	0.37	0.13

Table 2 Geo-nets and steel wire rope specifications [21, 22]

Reinforcement type	Product name	Tensile strength f_t	Yield point elongation YPE (%)	Shear stiffness (1 % drift) k_s (kN/m)	Mesh size l × b (mm)	Diameter ϕ (mm)
PET geo-net	Tencate Miragrid GX	38/38 kN/m	10/10	≈ 0/≈ 0	25 × 25	–
PP geo-net	Tenax RF1	9.3/17 kN/m	16/13	0.64/1.86	30 × 45	–
Steel wire ropes	–	1770 MPa	15	–	–	4

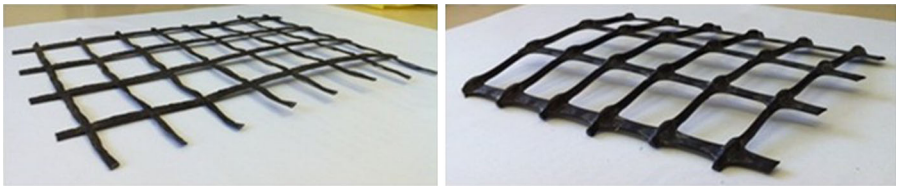

Fig. 1 Geo-nets used for strengthening of masonry walls (*left*—polyester, *right*—polypropylene)

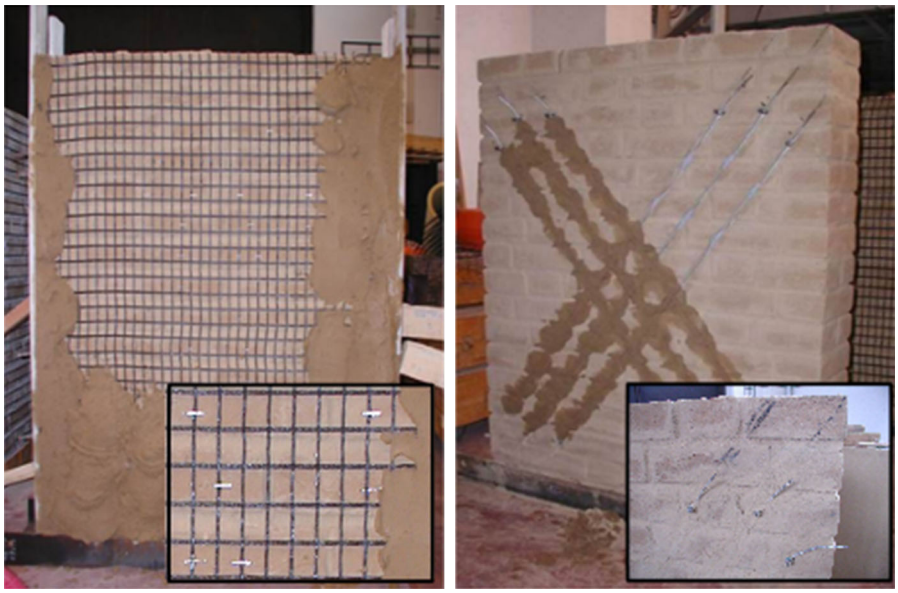

Fig. 2 Specimen strengthened using adobe plaster with PET geo-net (*left*; ABW-3) and steel wire ropes (*right*; ABW-2)

wall with a total of twelve wire ropes. First, three parallel grooves along each diagonal were made. Then the ropes were inserted into the grooves and each end of the rope was fastened to the wall with screws. The ropes were initially pre-stressed to 0.4 MPa, to ensure their effectiveness even at small displacements. Finally the grooves were filled with adobe mortar, to provide the coupling between the rope and the masonry.

An overview of all tested specimens along with their descriptions are given in Table 3.

Table 3 Overview of the specimens

Material	Label	Intervention
Adobe brick	ABW-1	–
Adobe brick	ABW-2	Steel wire ropes
Adobe brick	ABW-3	PET geo-nets
Adobe brick	ABW-4	PET geo-nets (Retrofitted ABW-1)
Adobe brick	ABW-5	PP geo-nets
Unfired clay brick	DBW-1	–
Unfired clay brick	DBW-2	Steel wire ropes
Unfired clay brick	DBW-3	PET geo-nets
Unfired clay brick	DBW-4	PP geo-nets

2.3 Testing rig, loading and measurement set-up

The masonry specimens were mounted into a special testing rig that simultaneously enabled uniform compression and cyclic horizontal loading on the top of the tested wall; see Fig. 3.

Figure 4 shows a diagram of the specimen placed within the testing system. The vertical load was generated by three hydraulic pistons (jacks) and was uniformly redistributed by means of an adjusted steel C-beam—closed at either side—placed on top of the

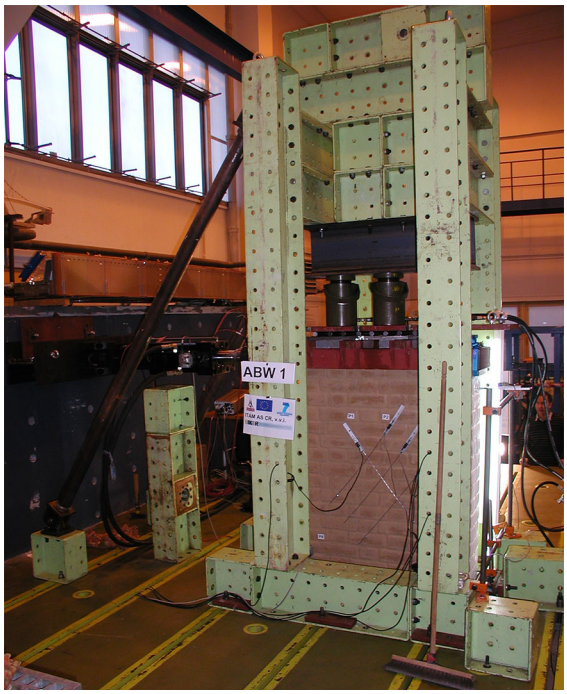

Fig. 3 Testing rig with the specimen

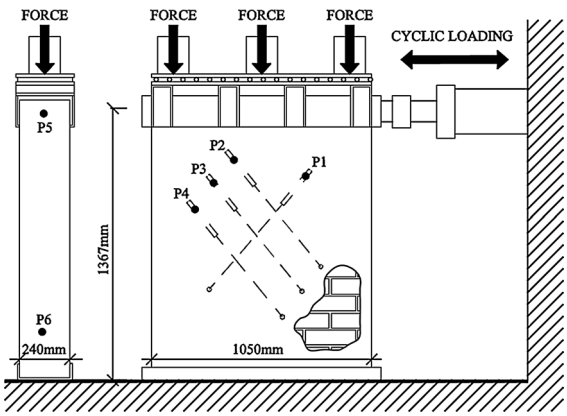

Fig. 4 Scheme of the testing system

wall. The load was controlled by means of the pressure of the hydraulic system within the jacks, which was manually kept at a constant value throughout the loading process. A horizontal displacement (force) at the top of the wall was introduced using a servo—hydraulic MTS actuator with a loading capacity of 250 kN.

During the experimental testing, the following loading conditions were considered. At first, only the above-mentioned compressive loading was applied. It was increased continuously up to a value of 80 kN, evenly distributed across the top cross section of the wall. Then, the vertical compressive pre-stress was combined with a cyclic horizontal loading mode with step-wise increments at each maximum cycle limit. The application of the horizontal load followed a triangular pattern with a constant frequency equal to 0.1 Hz. Three cycles for each step of the loading, defined by a maximum value of the amplitude of the displacement (starting from 2.5 mm and with increments of 2.5 mm) imposed by the actuator, were carried out. During the test, the forces on the vertical hydraulic jacks as well as on the horizontal actuator were recorded. The horizontal displacements at the bottom and the top of the wall and diagonal deformations on the surface were measured. The locations of the four diagonal (P_1, P_2, P_3 and P_4) and two horizontal LVDT sensors (P_5 and P_6) are shown in Fig. 4. The sequence of initiation and development of cracks in both surfaces was photography recorded during all loading steps. The loading was terminated when the total collapse of the specimen occurred or when there was a danger of uncontrollable collapse.

3 Evaluation methods

3.1 Procedure for evaluation of the bilinear curve

The actual hysteresis behaviour of a masonry wall, subjected to the combination of constant vertical load and a sequence of lateral loads, can be interpreted by the commonly used bilinear curve, see [23, 24] or [25] and Fig. 5.

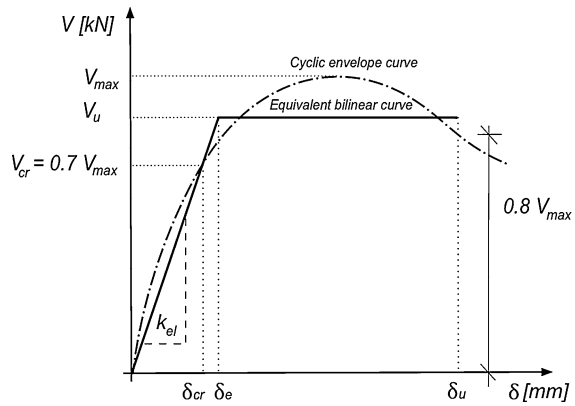

Fig. 5 Hysteresis envelope and its bilinear idealisation

The construction of a cyclic envelope of the hysteresis loops was carried out first. In the present case, the hysteresis loop represents a dependence of the horizontal force V (force of the actuator) on the top wall displacement δ (actuator displacement) for one cycle of the loading step. The characteristic value of the maximum force and the displacement were taken as averages of their maxima relative to the positive and negative loading directions. Three envelope curves, each corresponding to individual cycles, were constructed.

The parameters of the bilinear curve were determined using the following procedure. The first step was the evaluation of the elastic stiffness. The elastic stiffness k_{el} was obtained by drawing the secant to the experimental envelope at 70 % of V_{max} relative to the displacement δ_{cr} for which the development of the first cracks was expected:

$$k_{el} = \frac{0.7\ V_{max}}{\delta_{cr}} \tag{1}$$

Here, V_{max} denotes the maximum lateral force of the envelope curve. The second step consisted of estimating the ultimate displacement (δ_u). The ultimate displacement of the envelope curve is defined as the displacement corresponding to a strength degradation equal to 20 % of V_{max}. If this limit strength degradation is not reached, the ultimate displacement is assumed equal to the maximum obtained displacement.

Ensuring that the areas below the cyclic envelope curve (evaluated numerically as a sum of discrete areas A_i) and below the equivalent bilinear curve are equal, then:

$$\begin{aligned} A_{env} &= A_{bil} \\ \Sigma A_i &= V_u\ \delta_u - \frac{V_u^2}{2\ k_{el}} \end{aligned} \tag{2}$$

The value of the shear V_u corresponding to the horizontal branch of the bilinear curve takes the following form:

$$V_u = k_{el}\left[\delta_u - \sqrt{\delta_u^2 - \frac{2\ A_{env}}{k_{el}}}\right] \tag{3}$$

Knowing the elastic stiffness k_{el} and the value of V_u, it is possible to evaluate the elastic displacement δ_e:

$$\delta_e = \frac{V_u}{k_{el}} \tag{4}$$

Three bilinear curves, each corresponding to a particular envelope curve, were constructed. To obtain only one equivalent bilinear curve, the following procedure was carried out.

The equivalent ultimate displacement was assumed as the lowest of the ultimate displacements in each of three cycles computed as described here and similarly to the procedure in [26]:

$$\delta_{u,eq} = \min\left(|\delta_{u,1}|; |\delta_{u,2}|; |\delta_{u,3}|\right) \tag{5}$$

The equivalent elastic displacement δ_e and the equivalent value of V_u were assumed as the mean of values corresponding to particular cycles given by:

$$\delta_{e,eq} = \text{mean}\left(|\delta_{e,1}|; |\delta_{e,2}|; |\delta_{e,3}|\right) \tag{6}$$

resp.

$$V_{u,eq} = \text{mean}\left(|V_{u,1}|; V_{u,2}|; V_{u,3}|\right) \tag{7}$$

The equivalent ultimate ductility is defined as the ratio between the ultimate displacement and the elastic displacement:

$$\mu_u = \frac{\delta_{u,eq}}{\delta_{e,eq}} \tag{8}$$

Finally the value of the equivalent elastic stiffness was computed with the following expression:

$$k_{el,eq} = \frac{V_{u,eq}}{\delta_{e,eq}} \tag{9}$$

3.2 Method for evaluation of the energy dissipation

One of the most important factors which influences the seismic resistance of the structure is its damping property, or rather the mechanism of energy dissipation, which is the result of irreversible processes taking place in inhomogeneous systems. The effective dissipation of the energy by a structural element could significantly reduce the level of the vibration of the whole structure and decrease the effect of internal forces.

In this article, the dissipative properties of the analysed brick walls were expressed as a function of the area of the hysteresis loop. The loss factor η used for the assessment of the energy dissipation was

calculated from the following relation according to [27]:

$$\eta(\delta) = \frac{1}{n}\sum_{i=1}^{n}\frac{\Delta A_i(\delta)}{2\pi\, U_{\max,i}(\delta)} \tag{10}$$

This formula is actually the arithmetic mean over i loading cycles of the values representing the specific damping capacity per radian of the i-th loading cycle at given displacement δ. The term ΔA_i denotes the area of the hysteresis curve corresponding to i-th loading cycle, while $U_{\max,i}$ is the maximum potential energy of the system given by:

$$U_{\max,i}(\delta) = 1/2\, k_i(\delta)\, \delta^2 \tag{11}$$

where k_i is the actual stiffness of the wall taken as the slope of the corresponding hysteresis loop.

4 Experimental analysis of wall segments

In the following section, the results and the interpretation of the experimental tests on masonry brick walls, in terms of the load-carrying and deformation capacity, are presented. Particular attention is paid to the equivalent ultimate force $V_{u,eq}$ and the equivalent ultimate and elastic displacement $\delta_{u,eq}$ and $\delta_{e,eq}$ respectively, obtained from the bi-linearisation of the experimental shear—displacement envelopes. Additionally, the resulting ductility ratio μ_u was evaluated. The deformation parameters are normalised by the wall height, i.e. they are expressed in the form of top wall drift, for reasons of comparison.

4.1 Earth brick walls

The experimental campaign started with the tests on the unstrengthened wall, representing a control specimen. Figure 6 shows the elliptically-shaped hysteresis loops which were typical for all tested specimens. Only the loops corresponding to the first cycle of the loading steps are depicted, and loops related to different amplitudes of the controlled displacement are distinguished by color. The decreasing slope angle of the loops with increasing drift implies a decrease in the stiffness of the wall. The loops corresponding to all loading cycles are for the selected loading steps depicted in Fig. 7. The individual cycles are distinguished by line style. The reduction in maximum lateral force with increasing loading cycle number is clearly visible.

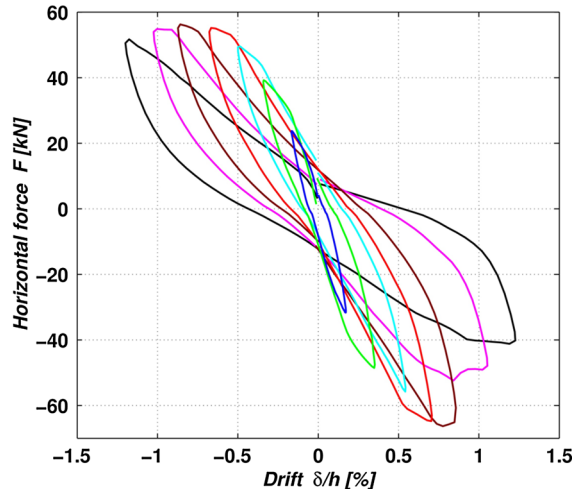

Fig. 6 Hysteresis loops of the unstrengthened adobe wall relative to the first cycle of different loading steps

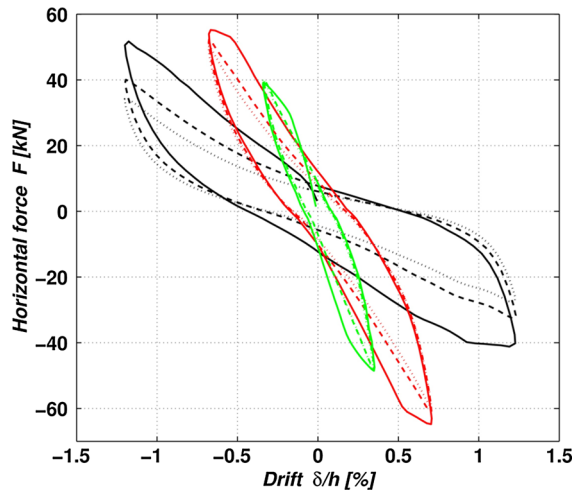

Fig. 7 Hysteresis loops corresponding to all cycles of selected loading steps of the unstrengthened adobe wall

The graph in Fig. 8 represents the envelope of the loops for each loading cycle together with their approximation to an idealised bilinear curve. The differences between the points on the envelope curves, corresponding to the same drift, pointed out a horizontal force degradation. In general, the force necessary to achieve the same drift decreased with the recurrence of the loading cycle. When the differences in the drift start to increase, this can be considered as

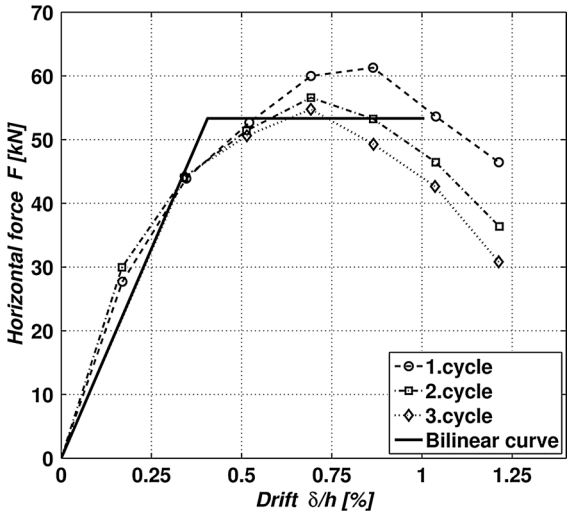

Fig. 8 Bilinear curve and envelope curves of the individual cycles of an unstrengthened adobe wall

the starting point of significant structural change, i.e. the first damage. Even though adobe is in general a brittle material, the horizontal part of the resulting bilinear curve demonstrated a slightly ductile behaviour.

The parameters of the bilinear curve of the unstrengthened specimen and their changes due to different intervention techniques were summarised in Tables 4 and 5, respectively. A crack distribution pattern, typical of that of a shear failure, formed on the wall surfaces during the loading process. The distribution pattern was characterised by cracks located along the diagonals of the wall, see Fig. 9. The first visible cracks were detected at a drift equal to 0.35 % (green curve in Fig. 6), which was considered as the initiation point of the divergence of the envelope curves related to the particular cycles.

The evaluation of the results from the tests carried out on the adobe wall strengthened with wire ropes, showed a substantial increase of the load carrying capacity of the wall in comparison to the control specimen, see Tables 4 and 5. The constructed bilinear curve and the corresponding envelope curves are shown in Fig. 10. An approximately two-fold increase in ultimate horizontal force was recorded. The effectiveness of the strengthening system is evident and is expressed as the increase in the displacement capacity of the wall. Also, a near doubled extension of the elastic region was achieved whilst keeping the equivalent stiffness at almost the same value as for the unstrengthened condition. The plastic part of the bilinear curve remained almost unchanged even though the ductility was decreased by about 30 %. The crack pattern consisted mainly of diagonal shear cracks, accompanied by vertical cracks, see Fig. 11. Damage in the lower corners of the wall, close to the point of the rope anchorage, was observed. Cracks that were caused by the higher concentration of the stresses, i.e. crushing of the corner, contributed to the detachment of the anchorage from the wall and prevented a composite action of rope and wall.

Another important aspect which was brought to light by the experiments was related to the damage due to the occurrence of out-of-plane movement of the strengthening elements. During the application of the cyclic horizontal loading the grooves with ropes were subjected to compression. This initiated the movement

Table 4 Parameters of bilinear curve of all analysed walls

Specimen	Material	Intervention	Elastic drift $\delta_{e,eq}/h$ (%)	Ultimate drift $\delta_{u,eq}/h$ (%)	Ductility u_u (−)	Ultimate force $V_{u,eq}$ (kN)	Elastic stiffness $k_{el,eq}$ (kN/mm)
ABW-1	Adobe	None	0.41	1.01	2.48	53.34	9.61
ABW-2	Adobe	Wire ropes	0.92	1.55	1.68	102.13	8.10
ABW-3	Adobe	PET geo-nets	0.75	1.27	1.69	72.20	7.05
ABW-4	Adobe	PET geo-nets (Retrofitting)	0.64	1.04	1.62	48.96	5.57
ABW-5	Adobe	PP geo-nets	0.89	1.49	1.67	78.75	6.46
DBW-1	Unfired clay	None	0.45	0.78	1.72	62.18	10.01
DBW-2	Unfired clay	Wire ropes	0.58	0.94	1.62	55.28	6.95
DBW-3	Unfired clay	PET geo-nets	0.50	0.96	1.94	61.79	9.13
DBW-4	Unfired clay	PP geo-nets	0.52	1.09	2.09	78.28	10.96

Table 5 Variation of the parameters of bilinear curve of walls due to interventions

Specimen	Material	Intervention	Elastic drift $\Delta\delta_{e,eq}$ (%)	Ultimate drift $\Delta\delta_{u,eq}$ (%)	Ductility Δu_u (%)	Ultimate force $\Delta V_{u,eq}$ (%)	Elastic stiffness $\Delta k_{el,eq}$ (%)
ABW-2	Adobe	Wire ropes	127	54	−32	91	−16
ABW-3	Adobe	PET geo-nets	85	26	−32	35	−27
ABW-4	Adobe	PET geo-nets (Retrofitting)	59	3	−35	−8	−42
ABW-5	Adobe	PP geo-nets	120	48	−33	48	−33
DBW-2	Unfired clay	Wire ropes	28	21	−5	−11	−31
DBW-3	Unfired clay	PET geo-nets	9	23	13	−1	−9
DBW-4	Unfired clay	PP geo-nets	15	40	22	26	10

Fig. 9 Crack pattern at failure of the unstrengthened adobe wall

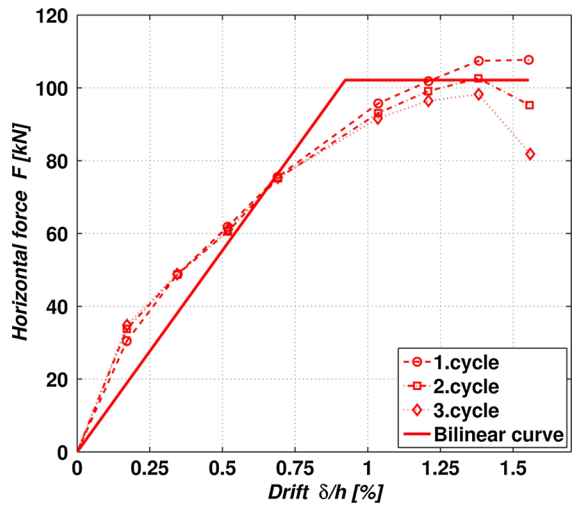

Fig. 10 Bilinear curve and envelope curves of the individual cycles of the adobe wall strengthened with wire ropes

of the ropes away from their grooves (as can be seen in Fig. 11), thereby decreasing the area of the cross-section of the wall withstanding the load. The occurrence of this phenomenon decreased the effective thickness of the wall and promoted the development of the major shear cracks along the diagonals. Although the ropes are still partially active, the mechanism of the transfer of forces is changed and the main stresses are transferred back onto the wall itself, following its diagonals. This, together with its decreased effective thickness—taking into account the empty grooves—initiated the development of the major diagonal shear cracks. The process of out-of-plane movement of the ropes and the above mentioned weakening also contributed to the rapid failure of the whole specimen.

The reinforcements using the mortar layer with both the PET and the PP geo-nets were found to improve the resistance of the wall against static vertical and cyclic horizontal loading. Figures 12 and 13 show the substitution of envelope curves by bilinear curves and Fig. 15 provides a comparison of the bilinear curves. The elastic range was widened in the top wall drift as well as along the vertical force axis. In this respect the usage of PP geo-net provided better efficiency, i.e. a greater increase in ultimate horizontal force (48 %) than with the application of the PET geo-net (35 %). Despite the higher tensile strength of the PET geo-net, the mesh of the PP geo-net was more rigid and was also reactive during its compression and

Fig. 11 Crack pattern (*left*), the out-of-plane deviation of the steel wire ropes (*top right*) and the damage of the corner (*bottom right*) near the rope anchor of a strengthened adobe brick wall

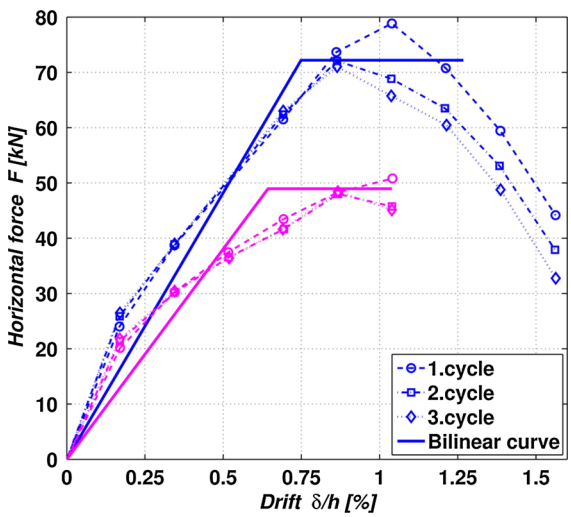

Fig. 12 Bilinear curve and envelope curves of the individual cycles of strengthened (*blue*) and retrofitted (*magenta*) adobe walls using PET geo-nets. (Color figure online)

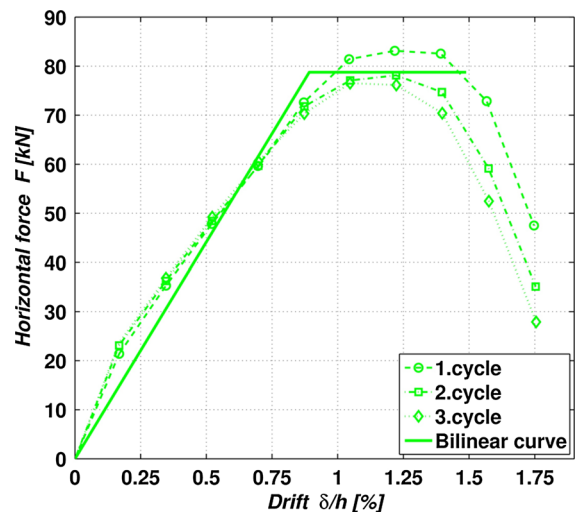

Fig. 13 Bilinear curve and envelope curves of the individual cycles of a strengthened adobe wall using PP geo-nets

so contributed more to the load carrying capacity. The rigidity of the PP geo-net can assure better distribution of the tension forces and therefore it can contribute to the increase of the total load-carrying capacity of the wall. Nevertheless, the improvement was lower than in the case of the wire ropes, see Tables 4 and 5. However, the ductility was reduced by about 30 %, which was similarly to the case with the ropes.

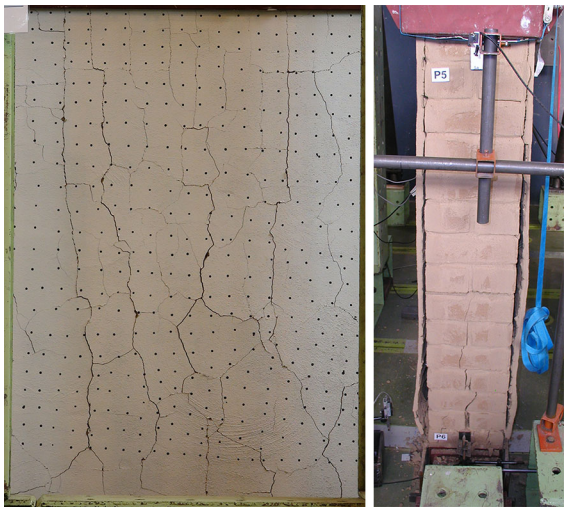

Fig. 14 Typical crack pattern (*left*) and detachment of the geo-nets with vertical cracks (*right*) in an adobe brick wall strengthened with PET geo-nets and adobe plaster

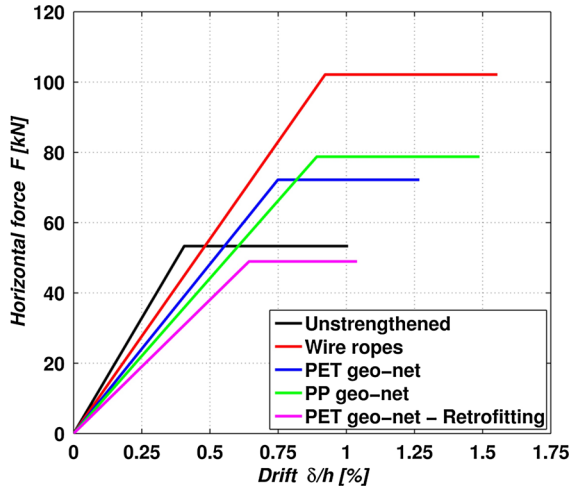

Fig. 15 Comparison of bilinear curves of all adobe walls

The applicability of PET geo-net with an adobe layer was also analysed for the purpose of partial retrofitting. The geo-net and the adobe layer were applied to the previously damaged, unstrengthened adobe wall (ABW 1) and tested in order to determine the parameters of the load carrying capacity. Subsequently, the results were compared with their counterparts in the undamaged and unstrengthened condition. In terms of the bilinear curve, the retrofitted wall had noticeably lower effective stiffness, lower horizontal ultimate force, longer displacement range of elastic behaviour and smaller ductility in comparison to the original control wall, see Fig. 15. The geo-net allowed not only the transfer and carrying of the tension forces by the geo-net but also ensured the integrity of the ruined wall. The analysis of the results revealed a high efficiency of retrofitting with the application of geo-nets, to ensure sufficient resistance of a totally damaged wall against in-plane cyclic loading and vertical compression.

More widespread and diffused cracks were observed on the surface of the walls receiving geo-nets and adobe plaster in comparison to the common shear failure cracking, see Fig. 14. The application of the geo-nets and the plaster resulted in the redistribution of the stresses originating from loading onto the two diagonal lines of the wall, thereby spreading the pattern over a wider area of the wall surface. The cracks visible on the surface represented a combination of two sets of damages: the first being masonry cracks and the second being cracks that occurred in the plaster only and originated from the differential movement of the geo-net mesh. The vertical crack in the middle of the thickness, at the bottom of the wall (as can be seen in Fig. 14 (right)) indicated the influence of the rocking mechanism on final failure of the whole specimen.

Another important aspect is the possible detachment of the geo-net from the masonry substrate, which could be expected especially when there is a difference in the stiffness between the strengthening materials and the material of the wall. This is particularly valid for the application of this kind of strengthening method to fired clay brick walls. In the case of the adobe material, the plaster is made of the same material as the bricks and therefore adhered better to the substrate, helping to keep the geo-nets in place.

Figure 15 compares the bilinear curves of all tested adobe walls, showing the efficiency and the impact of each particular intervention on the elastic as well as the plastic region.

The changes of the actual stiffness of the walls, i.e. the slope of the hysteresis loops with increasing drift, are depicted in Fig. 16. A decreasing tendency can clearly be observed for all walls, all following a similar trend. A comparison of the relationships between dashed lines, representing the equivalent elastic stiffness of the bilinear curves, and the relationships between solid lines, representing the actual stiffness, reveals some discrepancies. For instance, the actual stiffness of the wall with steel

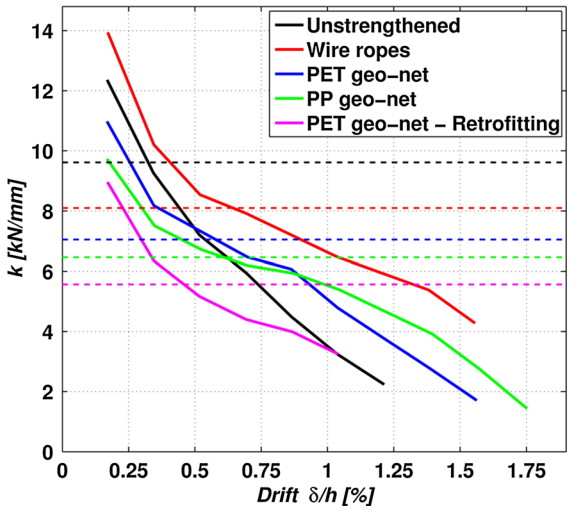

Fig. 16 Decrease of actual stiffness of tested adobe walls with increase of their drift (*dashed line*—the equivalent elastic stiffness of corresponding bilinear curve)

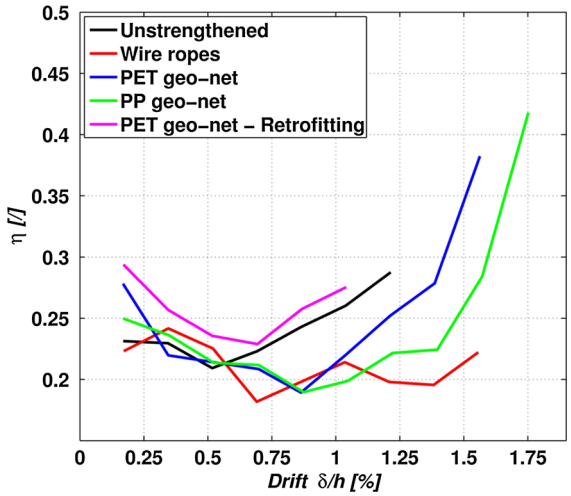

Fig. 17 Loss factor η of adobe walls as a function of drift

ropes was higher for all drift amounts than that of the unstrengthened specimen,which is contrary to the values of their equivalent elastic stiffness. This can be explained by the crude simplification when using the bilinear curve approximation. Also, slight changes in the overall motion of the wall may have contributed to the differences in stiffness. For example, the measured vertical uplift of the corners of the wall in the case of the strengthening using geo-nets was approximately 10 % higher than that in the case of the unstrengthened or strengthened walls with wire ropes and represented approximately 40 % of the current drift. The rocking mechanism affects the initial actual stiffness and also the evaluation of the equivalent stiffness. After a certain initiation period, including the hardening of the adobe, the actual stiffness followed the expected trend, i.e., higher stiffness for strengthened specimens. The reinforcement increased the resistance as well as the elastic range, however, it reduced the relative plastic behaviour, i.e., ductility, especially in the case of the adobe brick walls.

The loss factors η of all tested walls, representing damping capacity per unit angle of the cycle, showed similar trends with increasing top wall drift, see Fig. 17. The loss factor decreased slightly until the first significant damage occurred. Subsequently the damping increased, especially due to the friction in the cracks. This characterised the whole loading process until the total collapse of the specimens. The only exception was that of the intervention using steel ropes, for which the loss factor remained almost constant during the whole loading process due to a more effective redistribution of the tension forces in the wall body . In this case the tension forces were transferred to the ropes and fewer cracks (i.e. friction surfaces) were generated before the sudden collapse. As a result, the damping was lower than that of the unstrengthened specimen even after suffering the first considerable damage. The application of the geo-nets ensured integrity even after significant damage had occurred and thus achieved higher values of the loss factor at higher drifts. The geo-nets shifted the origin of the damping increase as well as the occurrence of the first visible damage, when compared with the unstrengthened wall, to a higher top wall drift values. The damping of the retrofitted wall with PET geo-nets was, for all drifts, higher than for the unstrengthened wall. The differences in lost factor were significant up to a drift of 0.75 %. Beyond this value, the loss factor was approximately equal to the factors of the unstrengthened state.

4.2 Unfired clay brick walls

A loading model identical to that used for the adobe walls was also applied to the walls built from unfired clay bricks. The evaluated results from the experimental measurements of the unstrengthened specimen revealed a higher load carrying capacity, nearly identical elastic stiffness and lower ductility in

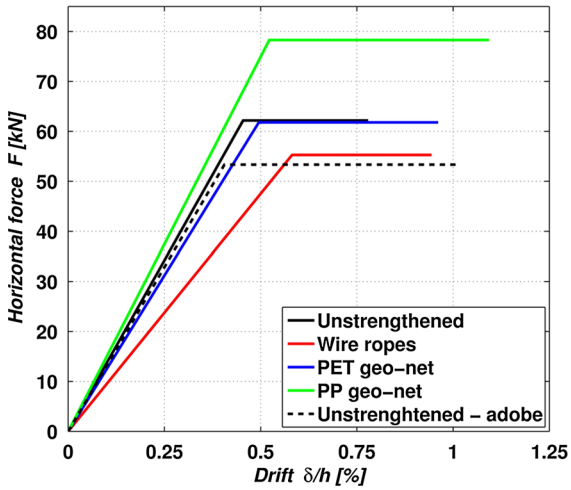

Fig. 18 Comparison of bilinear curves of all unfired clay brick walls

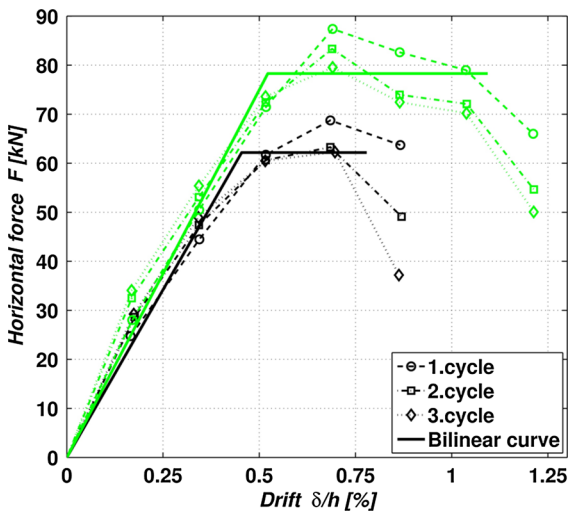

Fig. 19 Bilinear curve and envelope curves of the individual cycles of unstrengthened (*black*) and strengthened (*green*) unfired clay brick walls using PP geo-nets. (Color figure online)

comparison with the unstrengthened adobe wall, see Fig. 18. This supports the assumption of the adobe being a more plastic or ductile material. The construction of the bilinear curve from envelope curves is displayed in Fig. 19. Additionally, the actual stiffness of the unfired clay brick wall, obtained from the slope of the hysteresis loops, decreased with increasing top wall drift, see Fig. 20. The actual stiffness was almost the same as of the adobe wall.

The loss factor, i.e. damping, of the unstrenghtened unfired clay brick wall remained nearly constant until

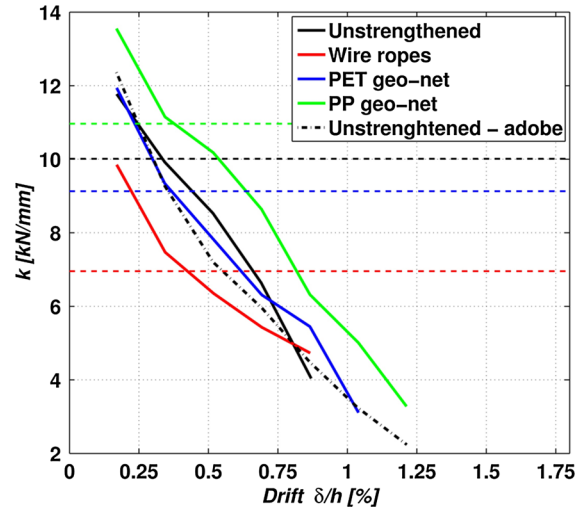

Fig. 20 Decrease of actual stiffness of tested unfired clay brick walls with increase of their drift (*horizontal dashed lines*—the equivalent elastic stiffness of bilinear curves of these unfired clay brick wall)

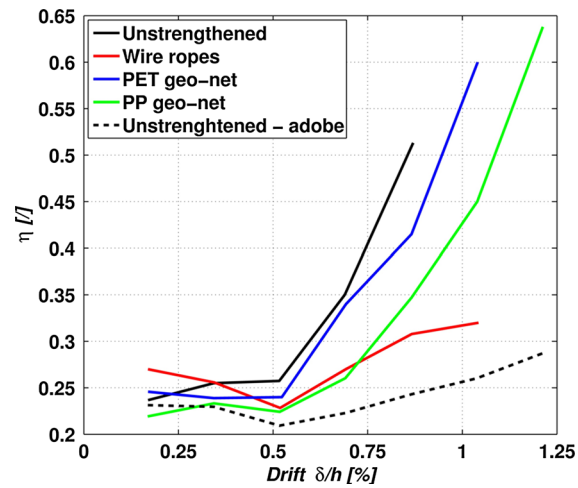

Fig. 21 Loss factor η of unfired clay brick walls as a function of drift

the first significant damage, see Fig. 21. Beyond this point, considerably higher damping was detected. The failure mode was characterised mainly by shear cracks located on each diagonal of the wall, see Fig. 22.

The application of the investigated intervention techniques to the unfired brick walls showed varying levels of success in comparison with their success observed for the adobe walls.

The strengthening using PP geo-nets led to an increase of the effective ultimate horizontal force and a moderate increase of the effective stiffness and elastic range, see Figs. 18 and 19. A comparison of bilinear curves corresponding to the adobe and the unfired clay brick walls with PP geo-nets showed approximately the same ultimate horizontal force, see Table 4. This would imply that the PP geo-nets are the main factor determining the limits of the horizontal force, neutralising the differences between the different walling materials. It also revealed that the additional plaster layer only had a minor influence. After strengthening, the ductility of the unfired brick wall increased, in contrast to decrease observed for adobe, by 22 % . The slope of the hysteresis loops, i.e. the actual stiffness of the wall, was higher than in the case of the unstrengthened unfired clay brick specimen, see Fig. 20. This was similar to the unstrengthened adobe wall, where the stiffness decreased with increasing drift and damage of the wall. However, the trend of the stiffness is more natural (higher for strengthened case) compared to the adobe wall; the influence of the consolidation process and the rocking mechanism were not significant. A similar shear failure mode, with the typical diagonal masonry cracks, can be seen in Fig. 22.

The tests on the walls with PET geo-nets and wire ropes have revealed the shortcomings of these strengthening systems. The importance of a secure connection between the inserted or attached strengthening elements and the wall was confirmed. The intervention using PET geo-nets proved to be inefficient due to an insufficient number and the weak anchorage of the steel staples. During the loading process, the PET geo-nets and the plaster detached easily and quickly from the surfaces of the masonry wall and prevented the transfer of the load to the geo-nets. The behaviour of the wall under loading remained the same as in the unstrengthened case, however, the plastic range of the bilinear curve subtly increased, see Fig. 18.

A similar problem occurred in the case of the intervention using wire ropes. The mortar applied to secure the ropes in their grooves failed to bond well with the bricks despite the fact that the grooves had been made sufficiently damp prior to application in order to ensure optimal adhesion. The ropes therefore disengaged from the grooves during their

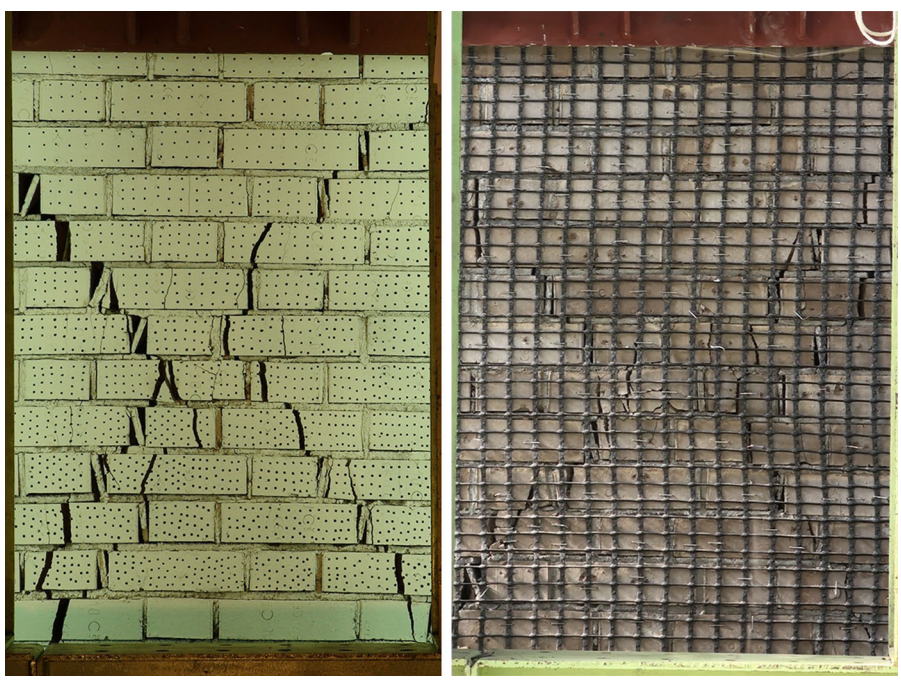

Fig. 22 Crack pattern at failure of unfired clay brick walls; (*left*) unstrengthened control specimen, (*right*) specimen strengthened using PP geo-nets

compression, causing not only an inefficiency of the intervention technique but also the weakening of the cross section of the wall which resisted the loading. This resulted in a decrease of the load-carrying capacity of the wall even below that of the unstrengthened specimen, see Fig. 18.

The trend of loss factor of all strengthened unfired clay brick walls follows trend of their counterparts from adobe, see Fig. 21 and compare with Fig. 17. Also in this case the application of the geo-nets ensured better integrity of the damaged wall and thus achieved higher values of the loss factor at higher drifts. The factor of the wall strengthened using wire ropes was also almost constant and was lower than for the unstrengthened specimen.

5 Conclusions

The paper has considered the interpretation of experimental lateral cyclic tests on earth and unfired clay brick masonry. The built specimens, loaded by a combination of constant vertical compressive prestress and a sequence of horizontal loadings, were tested under both unstrengthened and strengthened conditions. Two types of strengthening techniques were adopted for the wall surfaces. The first comprised of an additional mortar layer with geo-nets (polyester and polypropylene) and the second used steel wire ropes installed within grooves that were cut into the walls. The experimental data from the tests were analysed in terms of the load-carrying and the deformation capacity, and also the energy dissipation. Relevant parameters were determined from the bilinear curves constructed from the cyclic envelopes of the hysteresis loops or directly from the individual loops in the case of the damping evaluation. The evaluation of experimental results was based on bilinear curve approximation. It provides clear and physically meaningful parameters to describe both the elastic and the plastic behaviour of the tested walls under a combination of constant vertical and cyclic horizontal load. The authors consider this method to be designer-oriented, despite the omission of the exact knowledge of the full loading-displacement path.

The pilot tests on the unstrengthened specimens of both materials revealed their differences in mechanical behaviour. A lower load capacity but a higher deformation capacity and ductility was observed in the earthen masonry, in comparison to the unfired clay bricks, which reflects the different physical, mechanical and material characteristics of both structural elements. The application of all intervention techniques on the earth brick walls demonstrated a significant increase of the maximum force, as well as the maximum deformation they could withstand. The steel wire ropes were the most effective in these aspects, achieving an almost double ultimate lateral force and extension of the elastic region in comparison with the unstrengthened condition. Only slightly smaller increases were obtained for the walls strengthened with the mortar layer and geo-nets. On the other hand, unlike the more invasive strengthening with wire ropes, the geo-net also ensured integrity of the partly damaged wall. In addition, they were successfully applied to retrofit and to ensure a sufficient resistance of a previously ruined earth brick wall. The displacement range of the equivalent plastic behaviour remained almost constant for all tested specimens. Only the origin was shifted, due to interventions, towards a higher displacement. The comparison of bilinear curves corresponding to the earth and the unfired clay brick walls with polypropylene geo-nets showed approximately the same ultimate horizontal force. This indicates that geo-nets can be the major factor determining the limit of this parameter.

The tests with the unfired clay brick walls highlighted the shortcomings of the applied strengthening systems. The importance of ensuring the interconnection between the inserted or attached strengthening elements and the wall was confirmed. The intervention using PET geo-nets was inefficient due to detachment caused by an insufficient number and/or weak anchorage of the steel staples. A similar problem was observed in the case of wire ropes. The infill mortar did not sufficiently anchor the ropes in their grooves. Thus, the ropes became disengaged during their compression, which weakened the cross section of the wall and resulted in the decrease of the load-carrying capacity even below that of the unstrengthened specimen.

The analysis of the damping of both masonry types revealed similar trends, covering the same ranges and with increasing top wall displacement. The damping was either constant or slightly decreasing until the first significant damage occurred. Subsequently, the damping increased, mainly due to the friction in the cracks, until the moment of the total collapse of the

specimens. The only exception was that where steel ropes were used as an intervention method. In this case the damping remained near constant during the entire loading process.

Acknowledgments This work was supported by the Czech Science Foundation project No. 13-41574P, NIKER project (New integrated knowledge based approaches to the protection of cultural heritage from earthquake—induced risk), Grant Agreement no. 244123 and institutional support RVO 68378297.

References

1. Houben H, Guillaud H (1994) Earth construction: a comprehensive guide. ITDG Publishing, London
2. Silveira D, Varum H, Costa Á, Martins T, Pereira H, Almeida J (2012) Mechanical properties of adobe bricks in ancient constructions. Construction and Building Materials 28:36–44
3. Wu F, Li G, Li H, Jia J (2013) Strength and stress-strain characteristics of traditional adobe block and masonry. Materials and Structures 46:1449–1457
4. Angulo-Ibáñez Q, Mas-Tomás Á, Galvañ-LLopis V, Sántolaria-Montesinos JL (2012) Traditional braces of earth constructions. Construction and Building Materials 30:389–399
5. Tolles EL, Webster FA, Crosby A., Kimbro EE (1996) Survey of damage to historic adobe buildings after the January 1994 Northridge Earthquake. In: GCI Scientific Program Reports, The Getty Conservation Institute (eds.)
6. Croci G, D'Ayala D, D'Asdia P, Palombini F (1987) Analysis on shear walls reinforced with fibres. IABSE Symp. on Safety and Quality Assurance of Civil Engineering Structures, Tokyo
7. Triantafillou TC, Fardis MN (1997) Strengthening of historic masonry structures with composite materials. Materials and Structures 30:486–496
8. Triantafillou TC, Fardis MN (1993) Advanced composites for strengthening historic structures. IABSE Symp. on Structural Preservation of the Architectural Heritage, Rome, pp 541–548
9. Ehsani M, Saadatmanesh H, Al-Saidy A (1997) Shear Behavior of URM Retrofitted with FRP Overlays. Journal of Composites for Construction 1:17–25
10. Schwegler G (1994) Masonry construction strengthened with fiber composites in seismically endangered zones. In: Proceedings.of the 10th European conference on earthquake engineering, Vienna, Austria
11. Saadatmanesh H (1994) Fiber composites for new and existing structures. ACI Structural Journal 91(3):346–354
12. Ehsani MR (1995) Strengthening of earthquake-damaged masonry structures with composite materials. In: Taerwe L (ed) Non-metallic (FRP) reinforcement for concrete structures, pp 680–687
13. Papanicolaou CG, Triantafillou TC, Karlos K, Papathanasiou M (2007) Textile reinforced mortar (TRM) versus FRP as strengthening material of URM walls: in-plane cyclic loading. Materials and Structures 40(10):1081–1097
14. Papanicolaou CG, Triantafillou TC, Karlos K, Papathanasiou M (2008) Textile reinforced mortar (TRM) versus FRP as strengthening material of URM walls: out-of-plane cyclic loading. Materials and Structures 41(1):143–157
15. Papanicolaou CG, Triantafillou TC, Lekka M (2011) Externally bonded grids as strengthening and seismic retrofitting materials of masonry panels. Construction and Building Materials 25:504–514
16. Faella C, Martinelli E, Nigro E, Paciello S (2010) Shear capacity of masonry walls externally strengthened by a cement-based composite material: An experimental campaign. Construction and Building Materials 24:84–93
17. Prota A, Marcari G, Fabbrocino G, Manfredi G, Aldea C (2006) Experimental in-plane behavior of tuff masonry strengthened with cementitious matrixgrid composites. Journal of Composites for Construction 10(3):223–233
18. Aldea CM, Mobasher B, Jain N (2007) Cement-based matrix-grifd system for masonry rehabilitation, Textile Reinforced Concrete (TRC)—German/International Experience symposium sponsored by the ACI Committe 549, ACI Special Publications, SP-244-9, pp 141–156
19. Lehmsteine und Lehmmauermoertel, http://www.claytec.de/produkte/baustoffe/lehmsteine-und-lehmmauermoertel.html
20. Miccoli L, Müller U, Perrone C, Ziegert C (2012) Earth block masonry, rammed earth and cob: earthen components from different construction techniques and their structural performance. In: Proceedings of XIth international conference on the study and conservation of earthen architectural heritage, Lima, Peru
21. Miragrid GX—Geogrids (2009) Technical data, http://www.tencate.com
22. Tenax 3D Grids (2010) Technical data, http://www.tenax.net
23. Magenes G, Morandi P (2008) Proposal for the evaluation of the q—factor from cyclic test results of masonry walls. University of Pavia and Eucentre unpublished report, ESECMaSE project
24. Magenes G, Calvi GM (1997) In-plane seismic response of brick masonry walls. Earthquake Engineering and Structural Dynamics 26:1091–1112
25. Magenes G, Morandi P, Penna A (2008) Experimental in-plane cyclic response of masonry walls with clay units. In: Proceedings of the 14th world conference on earthquake engineering, Beijing, China
26. Frumento S, Magenes G, Morandi P, Calvi GM (2009) Interpretation of experimental shear tests on clay brick masonry walls and evaluation of q—factors for seismic design, Research Report No. 02.09, ESECMaSE project, University of Pavia and Eucentre
27. de Silva CW (2007) Vibration Damping, Control, and Design. CRC Press, Boca Raton, Florida, USA